DALTON
FULL PAPER

New Cu(I) and Ag(I) binuclear complexes containing the dppa ligand

Huizhang Liu,[a] Maria José Calhorda,[a,b] Michael G. B. Drew,[c] Vitor Félix,[d] Josef Novosad,[e] Luís F. Veiros,[f] Fabrizia Fabrizi de Biani[g] and Piero Zanello[g]

[a] *Instituto de Tecnologia Química e Biológica (ITQB), Av. da República, EAN, Apt 127, 2781-901 Oeiras, Portugal. E-mail: mjc@itqb.unl.pt*
[b] *Departamento de Química e Bioquímica, Faculdade de Ciências da Universidade de Lisboa, 1749-016 Lisboa, Portugal*
[c] *Department of Chemistry, University of Reading, Whiteknights, Reading, UK RG6 6AD*
[d] *Departamento de Química, Universidade de Aveiro, 3810-193 Aveiro, Portugal*
[e] *Department of Inorganic Chemistry, Faculty of Science, Masaryk University, Kotlárska 2, 611 37 Brno, Czech Republic*
[f] *Centro de Química Estrutural, Complexo I, Instituto Superior Técnico, Av. Rovisco Pais, 1, 1049-001 Lisboa, Portugal*
[g] *Chemistry Department, University of Siena, Via Aldo Moro, I-43100, Italy*

Received 5th September 2002, Accepted 24th September 2002
First published as an Advance Article on the web 30th October 2002

New Cu(I) and Ag(I) binuclear complexes were prepared by reaction of $[M(NCCH_3)_4][PF_6]$ (M = Ag, Cu) with the bidentate phosphine ligands $Ph_2PNHPPh_2$ (dppa) and $Ph_2PCH_2PPh_2$ (dppm). In the reaction of Cu(I) with dppa the phosphine is easily oxidized to give the octahedral species of $[Cu(dppaO_2)_3][PF_6]$, **1**. In an inert atmosphere, the binuclear complexes $[Cu_2(dppa)_2(NCCH_3)_3][PF_6]_2$, **2**, $[Cu_2(dppa)_2(NCCH_3)_4][PF_6]_2$, **3**, $[Ag_2(dppa)_2(NCCH_3)_2][PF_6]_2$, **4**, and $[Ag_2(dppm)_2][PF_6]_2$, **5**, were formed and structurally characterized by X-ray diffraction (except for **5**). The electrochemical studies showed that the most relevant property of the binuclear species was the ease of forming the metal upon reduction. EH and DFT calculations were performed in order to try and understand the structural features of the $[M_2(dppa)_2(NCCH_3)_x]^{n+}$ complexes, including the 0.47 Å increase in M ··· M distance upon going from **2** to **3**.

Introduction

The complexes of Cu(I) and Ag(I) containing bidentate phosphines have been widely studied, since these ligands can coordinate in a chelate or in a bridging mode, giving rise to a wide range of structures, some of them exhibiting interesting properties, such as luminescence.[1]

The role played by Cu(I) dimers as oxygen carriers in proteins, for instance haemocyanin, or as oxygen binders in cytochrome oxidase,[2] has added an extra interest to studying Cu(I) dimers. Cu(I) often adopts a tetrahedral coordination sphere, but other coodination geometries (linear and triangular) are possible, while for Ag(I) the lower coordination numbers are more frequently observed.[3] Binuclear species forming an eight-membered cycle have been described for the two cations when in the presence of a bidentate ligand, such as $Ph_2PCH_2PPh_2$ (dppm; Scheme 1),[4] and are also typical in Au(I) chemistry,

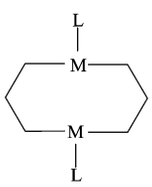

Scheme 1

although in this case the L ligand is usually absent.[5] The two metal atoms may be joined by a metal–metal bond, depending on the bridging ligand and the number of other ligands (L in Scheme 1) also attached to the metal.[6] The environment around each metal can be tuned by the number and bulk of these coligands.

In this work, M(I) cationic precursors (M = Cu, Ag) were used to prepare new derivatives of the $Ph_2PNHPPh_2$ (dppa) ligand and some dppm analogues, which were found to exhibit some interesting structural features. Their redox behavior was studied by cyclic voltammetry, and DFT[7] and EH[8] calculations were performed in order to rationalize the experimental findings.

Results and discussion

Chemical studies

The complex $[Cu(NCCH_3)_4][PF_6]$ was dissolved in dichloromethane and allowed to react with the bis(diphenyl)phosphinoamine ligand ($Ph_2PNHPPh_2$, dppa) 1 : 1. Different products were isolated depending on the reaction conditions. After filtration of the resulting product in air, white crystals were obtained by addition of hexane, after three days. The IR spectrum of this compound showed the band assigned to the ν_{N-H} vibration at 3292 cm^{-1} shifted relative to that of the free ligand (3229 cm^{-1}). The ^1H NMR spectrum in $NCCD_3$, although not very informative, indicated the presence of the phenyl protons between δ 7.13 and 7.30, as well as a singlet at δ 5.04, the N–H proton, integrating as 20 : 1. One peak assigned to the P atom of the coordinated ligand was observed in the ^{31}P NMR spectrum at δ 38.8, significantly shifted from that of the free ligand (δ 48.2). The structure of the compound was determined from a single crystal X-ray diffraction study to be $[Cu(dppaO_2)_3][PF_6]$, **1**, indicating that the ligand had been oxidized during the work up

DOI: 10.1039/b205922n

Table 1 Selected bond lengths (Å) and angles (°) for $[Cu(dppaO_2)_3]^+$, **1**

Cu(1)–O(2)	1.966(5)	Cu(1)–O(7)	2.133(5)
Cu(1)–O(6)	2.177(5)		
O(2)–Cu(1)–O(2a)	177.7(3)	O(2)–Cu(1)–O(7)	92.7(2)
O(2)–Cu(1)–O(7a)	89.0(2)	O(7)–Cu(1)–O(7a)	84.4(3)
O(2)–Cu(1)–O(6a)	90.8(2)	O(2)–Cu(1)–O(6)	87.7(2)
O(7)–Cu(1)–O(6a)	173.5(2)	O(7)–Cu(1)–O(6)	90.2(2)
O(6)–Cu(1)–O(6a)	95.4(3)		

Symmetry operator a: $-x + 3/2, -y + 1/2, z$.

and crystallization procedures. This formulation was in agreement with elemental analysis data. Oxidation of phosphine ligands in the presence of Cu(I) has been observed before, although to a smaller extent.[9]

A second batch was more carefully treated under nitrogen to prevent oxidation. The white precipitate was found to contain coordinated acetonitrile and dppa (IR and NMR data), but the elemental analysis was not consistent with the expected $[Cu_2(dppa)_2(NCCH_3)_2][PF_6]_2$ composition. The white product was thus recrystallized by slow diffusion of Et_2O into concentrated solutions of acetonitrile and acetone, giving two sets of crystals suitable for X-ray diffraction, which were subsequently identified as $[Cu_2(dppa)_2(NCCH_3)_3][PF_6]_2$, **2**, and $[Cu_2(dppa)_2(NCCH_3)_4][PF_6]_2$, **3**, respectively.

Each of these two complexes exhibited one signal in the ^{31}P NMR spectrum at δ 51.0 and 46.3, for **2** and **3**, respectively, reflecting the difference introduced by the fourth acetonitrile ligand in complex **3**. No effect of the asymmetry of **2** was detected. These values are much closer to the signal of the free ligand than in the case of the oxidized ligand in **1**.

A similar reaction occurred starting from the Ag(I) precursor, $[Ag(NCCH_3)_4][PF_6]$, and dppa. The white product was recrystallized by slow diffusion of Et_2O into a concentrated dichloromethane solution, affording white crystals suitable for X-ray diffraction. The ^{31}P NMR spectrum showed two peaks at δ 59.7 and 64.0, suggesting that the two P atoms of the ligand are no longer equivalent. This asymmetry was confirmed by the X-ray structure determination (details below), showing the complex to be $[Ag_2(dppa)_2(NCCH_3)_2][PF_6]_2$, **4**. Under the same conditions, the reaction of $[Ag(NCCH_3)_4][PF_6]$ and dppm led to the related compound, $[Ag_2(dppm)_2][PF_6]_2$, **5**, a species which has already been structurally characterized with another counter ion.[10]

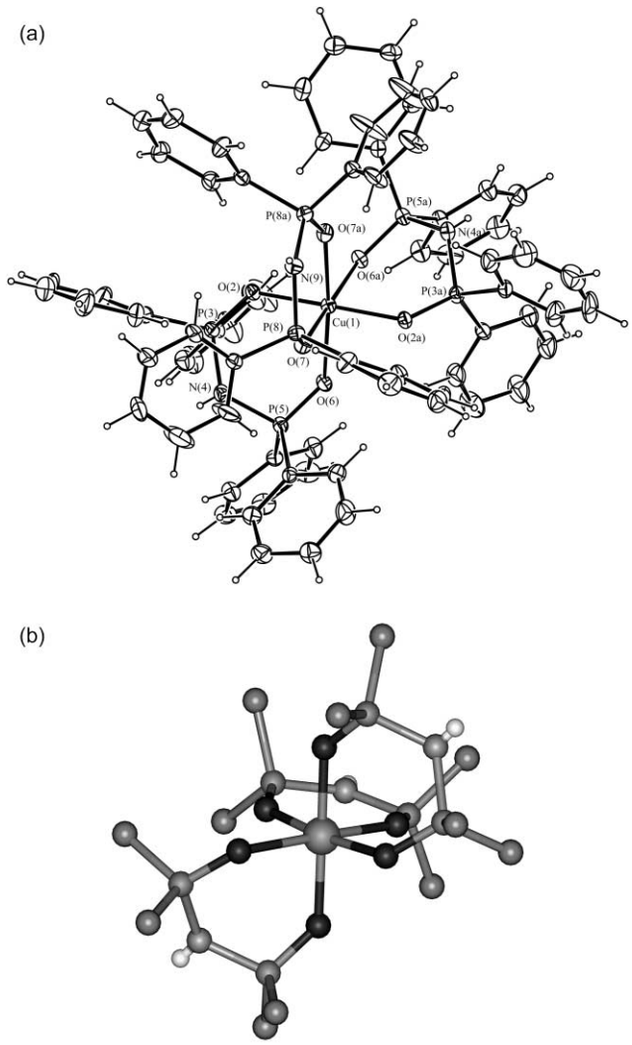

Fig. 1 Molecular diagrams of $[Cu(dppaO_2)_3]^+$, **1**, showing different structural features of the molecular structure. (a) ORTEP view showing the labelling scheme adopted and thermal ellipsoids drawn at the 10% probability level; (b) ball and stick representation showing the two-fold crystallographic axis. Only one carbon of the phenyl groups is shown for clarity.

Crystallography

The crystal structures of $[Cu(dppaO_2)_3][PF_6]$, **1**, $[Cu_2(dppa)_2(NCCH_3)_3][PF_6]_2$, **2**, $[Cu_2(dppa)_2(NCCH_3)_4][PF_6]_2 \cdot 2C_3H_6O$, **3**$\cdot 2C_3H_6O$, $[Ag_2(dppa)_2(NCCH_3)_2][PF_6]_2$, **4**, were determined by X-ray diffraction.

Fig. 1a shows an ORTEP diagram of the molecular structure of the complex cation $[Cu(dppaO_2)_3]^+$, **1**, with the labeling scheme adopted. The structure contains a two-fold crystallographic axis running through the copper centre and the N–H group comprising the nitrogen N(9). The copper is surrounded by six oxygen atoms from three oxidized dppa ligands with three independent Cu–O distances of 1.966(5), 2.177(5) and 2.133(5) Å. The molecular dimensions subtended at the copper centre, listed in Table 1, indicate that the coordination geometry is slightly distorted away from an ideal octahedron, as shown in Fig. 1b. The *cis* angles are within 5.4° of 90°, while the *trans* angles of 177.7(3) and 173.5(2)° are also close to the expected value of 180° for an ideal octahedron.

ORTEP diagrams of the dicationic species $[Cu_2(dppa)_2(NCCH_3)_3]^{2+}$, **2**, $[Cu_2(dppa)_2(NCCH_3)_4]^{2+}$, **3**, $[Ag_2(dppa)_2(NCCH_3)_2]^{2+}$, **4**, together with the labelling scheme adopted, are presented in Figs. 2a, 3a, and 4a.

In these three complexes, the two metal centres are held together by two dppa bridges, leading to the formation of a $M_2(PNP)_2$ cyclic eight membered framework. Selected bond lengths and angles found for these binuclear species are given in Table 2. An interesting structural feature is the different number of $NCCH_3$ ligands present in each complex, which ranges from two in **4**, to three in **2**, and four in **3**. The dicationic complex $[Cu_2(dppa)_2(NCCH_3)_3]^{2+}$, **2**, exhibits an asymmetric structure with the two copper centres having different co-ordination numbers, given by the number of acetonitrile ligands in their co-ordination spheres, one at Cu(5) and two at Cu(1), almost perpendicular, at an angle of 99.8(2)°. The 2.869(4) Å distance between the copper atoms is consistent with a weak metal–metal bonding interaction, leading to coordination numbers of five for Cu(1) and four for Cu(5), as discussed below. The co-ordination geometry of Cu(1) is pseudo square pyramidal, with the basal plane defined by the phosphorus atoms P(2) and P(8) from both dppa ligands, the nitrogen N(200) from an acetonitrile ligand, and the Cu(5) atom. The apical position is occupied by the nitrogen atom N(100) of the second acetonitrile ligand with a Cu–N(100) distance of 2.054(6) Å. The copper atom lies 0.480(2) Å above the mean least-squares plane [N(200), P(2), P(8), Cu(5)]. However, some angles centred at Cu(1) [139.8(1)° and 111.3(2)°] reveal an apparent distortion towards a bipyramidal geometry. The second copper centre, Cu(5), displays a distorted trigonal pyramidal environment with the basal trigonal plane formed by the two remaining

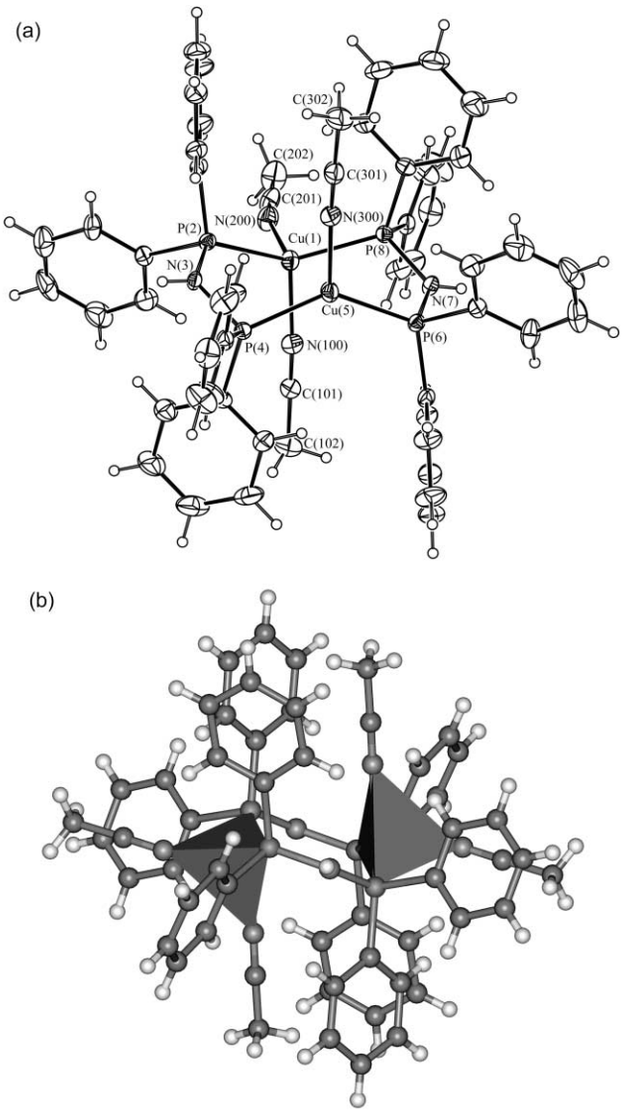

Fig. 2 Molecular diagrams of $[Cu_2(dppa)_2(NCCH_3)_3]^{2+}$, **2**, showing different structural features of the molecular structure. (a) ORTEP view showing the labelling scheme adopted and thermal ellipsoids drawn at the 30% probability level; (b) molecular representation emphasising the two $\{Cu_2N_2P_2\}$ interpenetrated pyramid co-ordination polyhedra, a square and a trigonal pyramid respectively.

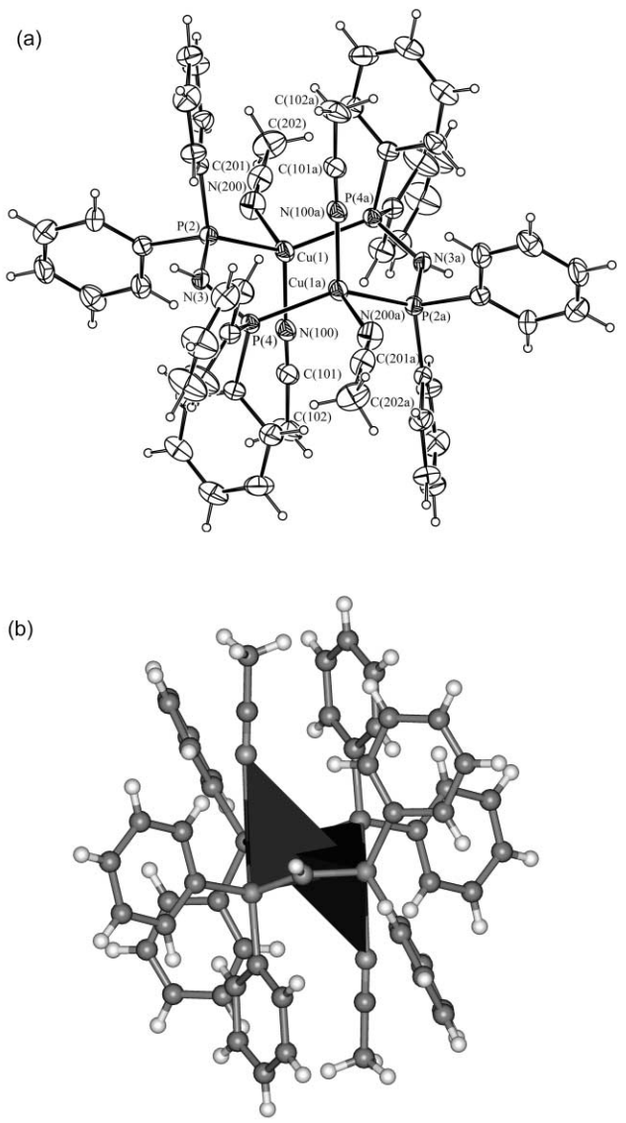

Fig. 3 Molecular diagrams of $[Cu_2(dppa)_2(NCCH_3)_4]^{2+}$, **3**, showing different structural features of the molecular structure. (a) ORTEP view showing the labelling scheme adopted and thermal ellipsoids drawn at the 20% probability level; (b) molecular representation showing the two independent $\{Cu_2N_2P_2\}$ trigonal pyramidal co-ordination polyhedra.

phosphorus atoms P(4) and P(6), from both dppa bridges, and N(300) of the unique acetonitrile ligand. The angles subtended at Cu(5) in the basal plane have the values of 106.6(2), 114.1(2) and 137.1(1)°. Cu(5) is only 0.182(2) Å away from the mean least-squares plane [P(4), P(6), N(300)]. The co-ordination polyhedra, a $\{Cu_2N_2P_2\}$ square pyramid and a $\{Cu_2NP_2\}$ trigonal pyramid, which interpenetrate, are seen in Fig. 2b.

The structure of the binuclear complex $[Cu_2(dppa)_2(NCCH_3)_4]^{2+}$, **3**, has C_i symmetry, with a crystallographic inversion localized at the midpoint of the two copper atoms. The distance between the two metal centres of 3.341(2) Å is too long for a M–M single bond to be assigned. The co-ordination sphere of each metal centre is pseudo trigonal pyramidal with the basal plane defined by two phosphorus donor atoms from different dppa ligands and one acetonitrile ligand. The fourth co-ordination is achieved by the nitrogen donor of the bent equatorial acetonitrile ligand [C(201)–N(200)–Cu(1) angle 150.7(10)°]. The apical acetonitrile is co-ordinated in a linearly [C(101)–N(100)–Cu(1) angle 177.8(7)°]. The co-ordination polyhedra comprise two $\{Cu_2N_2P_2\}$ trigonal pyramid units, as shown in Fig. 3b.

The complex $[Ag_2(dppa)_2(NCCH_3)_2]^{2+}$, **4**, has a crystallographic centrosymmetric structure, with the inversion centre localized at the midpoint of the two silver atoms. The dppa chelating ligands hold the silver centres at a distance of 2.961(3) Å, indicative of a M–M single bond. Thus, the co-ordination geometry around the silver centres can be also described as pseudo pyramidal trigonal, with the basal plane defined by the two phosphorus atoms from both dppa ligands and one acetronitrile ligand. The apical co-ordination site is occupied by the second silver centre, forming co-ordination polyhedra composed of two interpenetrated $\{Ag_2N_2P_2\}$ trigonal pyramids, as shown in Fig. 4b.

In order to compare the structures of the complexes studied with other similar ones, a search on the Cambridge Structural Database[11] was undertaken, using the cyclic $M_2(PXP)_2$ structural unit, where M is a copper or silver centre, and X a carbon or a nitrogen bridging atom. The molecular formulae of the binuclear complexes and CSD REFCODES as well as their relevant structural data for comparison purposes are given in Tables 3 and 4 for copper(I) and silver(I) species, respectively. The parameters listed comprise the displacements of the N or C atoms of the bridging ligands from the mean least-squares plane defined by the four phosphorus donors of the two dppa bridges and the two metal centres.

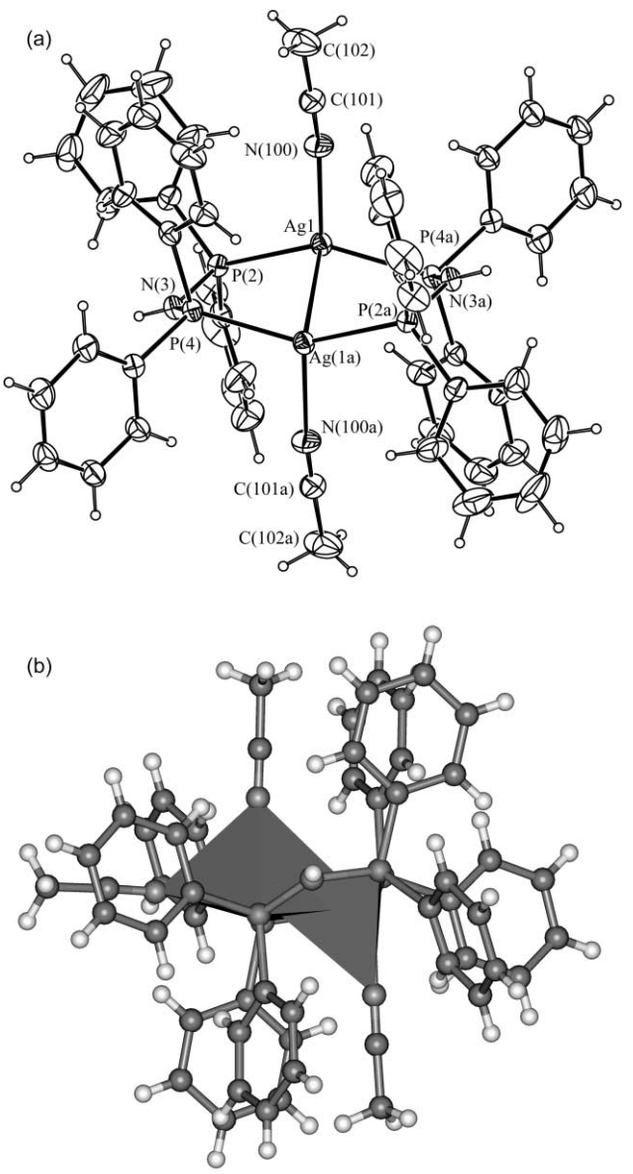

Fig. 4 Molecular diagrams of $[Ag_2(dppa)_2(NCCH_3)_2]^{2+}$, **4**, showing different structural features of the molecular structure. (a) ORTEP view showing the labelling scheme adopted and thermal ellipsoids drawn at the 20% probability level; (b) molecular representation showing the two interpenetrated $\{Ag_2N_2P_2\}$ trigonal pyramidal co-ordination polyhedra.

The relative positions of the two bridging atoms N or C relative to the P_4 plane give rise either to a boat-like arrangement, when these two atoms are on the same side of the plane, or a chair-like one, when they are on opposite sides. The complexes **2**, **3**, and **4** have chair-like conformations, which are imposed in the last two cases by the crystallographic symmetry (see above). This conformation is the most frequent among the remaining complexes listed in Tables 3 and 4, but there are also some examples of boat-like configurations. Furthermore, the complex $[Cu_2(dcpm)_2(NCCH_3)_2]^{2+}$, **6**, [dcpm = bis(dicyclohexyl)-phosphinomethane] displays a chair-like conformation, while the related $[Cu_2(dppm)_2(NCCH_3)_2]^{2+}$, **7**, exhibits a boat-like conformation, suggesting the role of steric effects (phenyl *vs.* cyclohexyl substituents).

The complexes in Tables 3 and 4 show a wider range of M ⋯ M distances for copper than for silver. The M ⋯ M distance in $[Cu_2(dppa)_2(NCCH_3)_3]^{2+}$, **2**, is only 0.06 Å longer than in $[Cu_2(dcpm)_2(NCCH_3)_2]^{2+}$, **6**, but almost 1 Å shorter than in $[Cu_2(dppm)_2(NCCH_3)_2]^{2+}$, **7**. The distance between the two metal centres (silver or copper) within the apparently rigid $M_2(PXP)_2$ framework reflects the presence of the other ligands in the metal co-ordination spheres, being governed by a delicate balance between the electronic requirements of the metal and the steric demands of the bulky ligands.

Electrochemistry

Cu(I) complexes **2** and **3** possess a rather similar redox propensity. As a typical example Fig. 5 illustrates the cyclic voltammetric profile of **3**.

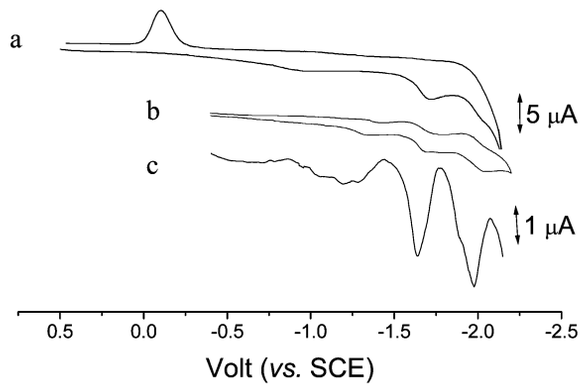

Fig. 5 Cyclic (a, b) and differential pulse (c) voltammograms recorded at a platinum electrode on a $NCCH_3$ solution of **3** (0.7×10^{-4} mol dm^{-3}). $[NEt_4](PF_6)$ (0.1 mol dm^{-3}) supporting electrolyte. Scan rates: (a) 0.2 V s^{-1}; (b) 0.05 V s^{-1}; (c) 0.02 V s^{-1}.

It undergoes two separate reduction processes, featuring partial chemical reversibility. In fact, at the scan rate of 0.05 V s^{-1} the i_{pa}/i_{pc} ratio for the two processes is about 0.5. On the other hand, the stripping peak appearing at −0.11 V in the backscan testifies to both the one-electron nature of each step and their ultimate chemical irreversibility. It is noteworthy that the same stripping peak can be recorded also inverting the potential scan after traversing the first reduction process, thus unambiguously allowing each process to be ascribed to the Cu^I/Cu^0 redox change. The presence of two well-separated redox changes in these structurally symmetric dimers suggests the existence of electronic communication between the two copper-based subunits. Based on the separation of the two reductions a K_{com} value of about 6×10^6, can be calculated for both complexes **2** and **3**, allowing the instantaneously electrogenerated Cu^ICu^0 congeners to be regarded as delocalized Robin–Day class III mixed-valent systems. The lack of the Cu(I)/Cu(II) redox change indicates the high stability of the Cu(I) complexes. This fact is in agreement with the presence of chemically oxidized *ligands* in **1**, obtained when the reactants are not worked up under nitrogen.

At variance with their Cu(I) congeners, the Ag(I) complexes **4** and **5** undergo a single two-electron reduction process, irreversible in character, Fig. 6.

Also in this case the anodic stripping peak which is observed in the backscan indicates the occurrence of a simultaneous Ag^I/Ag^0 redox change of the two silver-based subunits. Changing dppa for dppm simply causes a cathodic shift (by about 0.5 V) of the reduction process. From a speculative viewpoint the Ag^IAg^0 intermediate reduction products from **4** and **5** should belong to the localized Robin–Day class I. The redox potential values of compounds **2**–**5** are collected in Table 5.

Molecular orbital calculations

EH calculations[8] were performed on model complexes, $[Cu_2(PH_3)_4(HCN)_n]^{2+}$, $n = 3$ or 4, in order to interpret qualitatively the differences in Cu–Cu distances for complexes **2** and **3**, on the basis of the different coordination environments of copper atoms. Each chelate phosphine was replaced by two PH_3 groups, and hydrogen atoms were used instead of methyl groups. More details are given in the Computational details section. Both Cu atoms in **3** and one of them in **2** exhibit an

Table 2 Selected bond lengths (Å) and angles (°) for $[Cu_2(dppa)_2(NCCH_3)_3]^{2+}$, **2**, $[Cu_2(dppa)_2(NCCH_3)_4]^{2+}$, **3**, and $[Ag_2(dppa)_2(NCCH_3)_2]^{2+}$, **4**

$[Cu_2(dppa)_2(NCCH_3)_3]^{2+}$, **2**			
Cu(1) ··· Cu(5)	2.869(4)	Cu(5)–N(300)	1.998(6)
Cu(1)–N(100)	2.054(6)	Cu(1)–N(200)	2.098(6)
Cu(1)–P(2)	2.262(3)	Cu(1)–P(8)	2.274(3)
Cu(5)–P(4)	2.248(3)	Cu(5)–P(6)	2.241(4)
P(2)–Cu(1)–P(8)	139.8(1)	N(200)–Cu(1)–P(8)	96.5(2)
N(200)–Cu(1)–P(2)	97.1(2)	N(100)–Cu(1)–N(200)	99.8(2)
N(100)–Cu(1)–P(8)	103.4(2)	N(100)–Cu(1)–P(2)	111.3(2)
P(6)–Cu(5)–P(4)	137.1(1)	N(300)–Cu(5)–P(4)	106.6(2)
N(300)–Cu(5)–P(6)	114.1(2)	N(300)–Cu(5)–Cu(1)	101.4(2)
Cu(1)–Cu(5)–P(4)	88.9(1)	Cu(1)–Cu(5)–P(6)	95.7(1)
N(100)–Cu(1)–Cu(5)	92.5(2)	N(200)–Cu(1)–Cu(5)	166.8(2)
P(2)–Cu(1)–Cu(5)	82.5(1)	P(8)–Cu(1)–Cu(5)	76.0(1)
$[Cu_2(dppa)_2(NCCH_3)_4]^{2+}$, **3**			
Cu(1) ··· Cu(1a)	3.341(2)	Cu(1)–N(200)	2.242(10)
Cu(1)–N(100)	2.023(9)	Cu(1)–P(4)	2.264(3)
Cu(1)–P(2)	2.252(3)		
P(2)–Cu(1)–P(4a)	137.7(1)	N(100)–Cu(1)–N(200)	99.9(4)
N(100)–Cu(1)–P(2	111.8(2)	N(200)–Cu(1)–P(4)	94.5(3)
N(200)–Cu(1)–P(2)	95.4(3)	N(100)–Cu(1)–P(4)	106.7(2)
P(2)–Cu(1)–P(4)	137.7(1)		
$[Ag_2(dppa)_2(NCCH_3)_2]^{2+}$, **4**			
Ag(1)–Ag(1a)	2.961(3)	Ag(1)–P(4a)	2.450(3)
Ag(1)–N(100)	2.382(6)	Ag(1)–P(2)	2.436(3)
P(2)–Ag(1)–P(4a)	148.4(1)	N(100)–Ag(1)–Ag(1a)	104.8(2)
N(100)–Ag(1)–P(2)	110.7(2)	N(100)–Ag(1)–P(4a)	100.8(2)
P(2)–Ag(1)–Ag(1)	93.3(1)	P(4a)–Ag(1)–Ag(1a)	79.5(1)

Symmetry operators: For **3**: $-x + 1, -y + 2, -z + 2$; For **4**: $-x + 1, -y + 1, -z$.

Table 3 Structural data for $Cu_2(PXP)_2$ complexes, where X represents a bridging nitrogen or a carbon

Refcode	Compound	M–M/Å	D_1[a]/Å	D_2[a]/Å
This work	$[Cu_2(dppa)_2(NCCH_3)_3]^{2+}$, **2**	2.869(1)	0.30(1)	−0.33(1)
This work	$[Cu_2(dppa)_2(NCCH_3)_4]^{2+}$, **3**	3.341(2)	0.16(1)	−0.16(1)
FISZAI	$[Cu_2(dPr^ipm)_2Cl_2]$	2.973	0.63	−0.63
JOGNUO	$[Cu_2(dppm)_2(phen)_2]^{2+}$	4.742	0.74	−0.74
KIKBEL	$[Cu_2(dppm)_2(L)_2]^{2+}$	3.452	0.94	−0.33
LOVGUY[b]	$[Cu_2(dcpm)_2(ClO_4)_2]$	2.731	0.54	−0.54
		2.639	*0.47*	*−0.47*
LOVHAF	$[Cu_2(dcpm)_2(PF_6)_2]$	2.790	0.60	−0.60
LOVHEJ[b]	$[Cu_2(dcpm)_2I_2]$	2.938	0.54	−0.54
		2.872	*0.58*	*−0.58*
LOVHIN[c]	$[Cu_2(dcpm)_2(NCCH)_2]^{2+}$, **6**	2.810	0.60	−0.61
LOVHUZ[c]	$[Cu_2(dcpm)_2(NCCH_3)_2]^{2+}$, **6**	2.810	0.59	−0.59
SOMJAF	$[Cu_2(dppm)_2L_2]$	2.944	0.93	−0.29
SUHFIK	$[Cu_2(dppm)_2L_2]^{2+}$	3.865	0.90	−0.36
SULXUS	$[Cu_2(dppm)_2PhCO_2]$	3.359	0.73	−0.73
NICPIY	$[Cu_2(2\text{-}dppmpy)_2(THF)_2]$	3.372	0.89	−0.89
DEDFEX	$[Cu_2(dppm)_2(m\text{-}MePhS_2C)_2]$	3.426	1.02	−1.02
FEWVAE	$[Cu_2(dppm)_2(NCCH_3)_2]^{2+}$, **7**	3.757	0.97	−0.97
NIKBAK	$[Cu_2(dppm)_2(NO_3)_2]$	3.170	0.96	−0.96
NIKBAK02		3.170	0.95	−0.95
WAZXUQ	$[Cu_2(dBu^tpm)_2]^{2+}$	2.731	0.02	−0.02

[a] D_1 and D_2 are the displacement of X above and below, respectively, the P_4 mean least squares plane. [b] The values in italics correspond to the second molecule present in the asymmetric unit. [c] The crystal structure of $[Cu_2(dcpm)_2(NCCH_3)_2]^{2+}$ was determined twice with PF_6^- and ClO_4^- salts respectively.

almost square pyramidal environment, while the second Cu atom in **2** only coordinates to three donor atoms of the ligands. Therefore, although the d^{10} metal electronic configuration is the same and the entire d set is filled, the frontier orbitals differ in the two metals. Indeed, as the highest occupied levels are Cu–L antibonding orbitals, the smaller number of ligands attached to the metal on CuL_3 yields more stabilized fragment orbitals than for CuL_4.

Scheme 2 depicts, in a simplified way, the interaction between the two metallic fragments in the model complexes. The left side represents the interaction between the two $[Cu(PH_3)_2(HCN)_2]^+$ fragments in $[Cu_2(PH_3)_4(HCN)_4]^{2+}$, the model for complex **3**. Given the d^{10} metal electronic configuration, the entire d set is filled, and the HOMO of the CuL_4 fragments (1a) has a Cu–L antibonding character. The combination between those fragment orbitals results in a four electron destabilizing interaction, where s and p mixing provides some stabilization. Namely, there is a mixing of a metal *x* orbital (fragment orbital 2a, also Cu–L antibonding) into the complex HOMO, reducing its Cu–Cu antibonding character and stabilizing the interaction.

Table 4 Structural data for $Ag_2(PXP)_2$ complexes, where X represents a bridging nitrogen or a carbon

Refcode	Compound	M–M/Å	D_1[a]/Å	D_2[a]/Å
This work	$[Ag_2(dppa)_2(NCCH_3)_2]^{2+}$, **4**	2.961(1)	0.44(1)	−0.44(1)
BEPFOR	$[Ag_2(dmpm)_2]^{2+}$	3.042	0.55	−0.55
DEKXAS	$[Ag_2(dppm)_2(L)_2]$	3.846	0.77	−0.77
NAQMOH	$[Ag_2(dppm)_2]^{2+}$	2.953	0.74	−0.74
QICZUX	$[Ag_2(dcpm)_2]^{2+}$	2.959	0.60	−0.60
		2.934	*0.62*	*−0.62*
QIDBAG[b]	$[Ag_2(dcpm)_2]^{2+}$	2.937	0.68	−0.68
		2.907	*0.47*	*−0.47*
CEMXOH	$[Ag_2(dppm)_2(NO_3)_2]$	3.084	0.93	−0.93
GIYQAG	$[Ag_2(dppa)_2(THF)_2]^{2+}$	2.911	0.76	−0.76
YILBOK	$[Ag_2(dppm)_2(CH_3CO_2)]^{2+}$	3.194	0.74	−0.74
YIRNAO	$[Ag_2(dppm)_2(\{CF_3CO\}_2CH)]$	3.153	0.61	−0.61

[a] D_1 and D_2 are given in Table 3. [b] The values in italics correspond to the second molecule present in the asymmetric unit.

Table 5 Peak potential values (V, *vs.* SCE) for the redox changes exhibited by complexes **2**–**5** in $NCCH_3$ solution

Complex	$E^{\circ\prime}$[a] M^IM^I/M^IM^0	M^IM^0/M^0M^0
$[Cu_2(dppa)_2(NCCH_3)_3]^{2+}$, **2**	−1.6	−2.0
$[Cu_2(dppa)_2(NCCH_3)_4]^{2+}$, **3**	−1.7	−2.1
$[Ag_2(dppa)_2(NCCH_3)_2]^{2+}$, **4**	−1.10[b]	
$[Ag_2(dppm)_2(NCCH_3)_2]^{2+}$, **5**	−1.60[b]	

[a] Measured at 0.1 V s^{-1}. [b] Two-electron process.

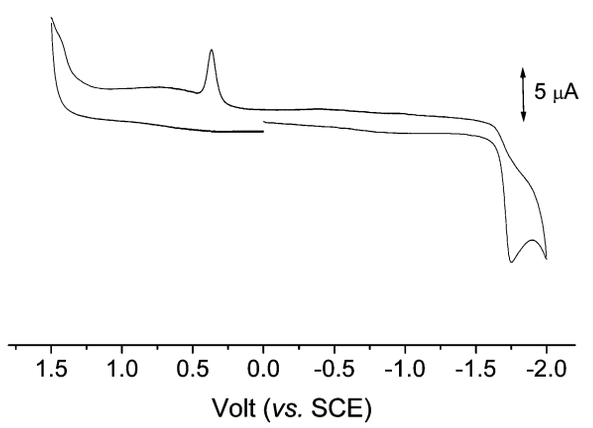

Fig. 6 Cyclic voltammogram recorded at a platinum electrode on a $NCCH_3$ solution containing $[NEt_4](PF_6)$ (0.1 mol dm^{-3}) and **4** (0.9×10^{-4} mol dm^{-3}). Scan rate: 0.2 V s^{-1}.

The overall result is a weak attractive interaction between the two fragments, shown by a 0.035 $[Cu(PH_3)_2(NCH)_2]^+$–$[Cu(PH_3)_2(NCH)_2]^+$ overlap population and a HOMO for the dimer with 8% participation of copper s and p orbitals. This is also shown by the population of the fragment molecular orbitals (FMO) involved in the bonding. There is a slight depopulation of FMO 1a, 1.97 electrons, and the corresponding population of FMO 2a (0.02 electrons).

The bonding between $[Cu(PH_3)_2(HCN)_2]^+$ and $[Cu(PH_3)_2(HCN)]^+$ in $[Cu(PH_3)_4(HCN)_3]^{2+}$ is represented on the right side of Scheme 2, and models the metal–metal interaction in complex **2**. In this case two different fragments interact, CuL_4 and CuL_3. The relevant FMO for CuL_3 are equivalent in nature to the ones previously discussed for CuL_4, the fragment HOMO, metal d (1a), and an empty metal *x* orbital, but the smaller number of ligands attached to the metal on the CuL_3 fragment yields more stabilized FMO (FMO 2a is *ca.* 1 eV more stable for CuL_3 than for its CuL_4 equivalent). The smaller energy difference between the CuL_4 HOMO (1a) and CuL_3 2a results in a stronger interaction between those orbitals. This leads to an increased electronic transfer between FMOs, the electronic populations becoming 1.95 for CuL_4 1a and 0.05 for CuL_3 2a,

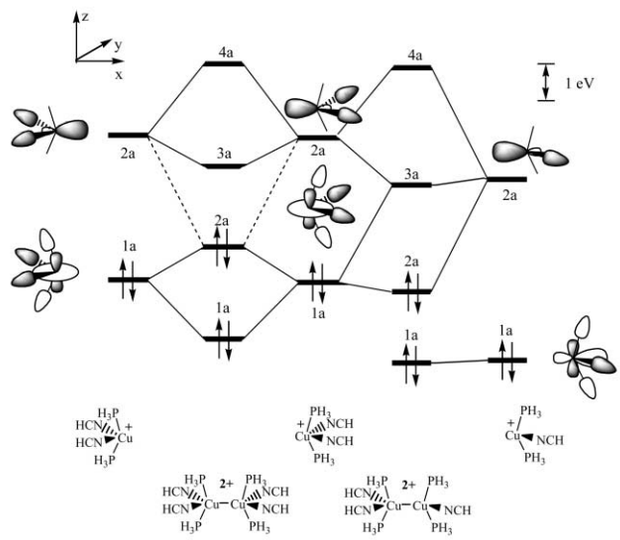

Scheme 2

and to a greater participation of metal s and p orbitals in the Cu–Cu bonding (the complex HOMO, 2a, has 19% copper s and p character). The result is a stronger Cu–Cu bond, as shown by the $[Cu(PH_3)_2(NCH)_2]^+$–$[Cu(PH_3)_2(NCH)]^+$ overlap population (0.049) and in accordance with the experimental Cu–Cu distances (2.87 Å for **2** and 3.34 Å for **3**). The relative energy order of the LUMOs is also in accord with the observed trend in the redox potential values, **2** being easier to reduce than **3**. Moreover, addition of an electron involves the occupation of a further CuL antibonding orbital and therefore this picture explains why on reduction these complexes decompose, losing the ligands and giving rise to free Cu.

This result parallels what was found for gold polynuclear mixed valence complexes, in which the Au–Au bond strength and the metal formal oxidation state are strongly dependent on the number of L ligands bonded to each Au atom.[6a]

DFT calculations[7] were performed using the B3LYP[12] approach in Gaussian 98 program.[13] The geometries of the models of the two Cu complexes **2** and **3** were fully optimized without any symmetry constraints. In the models, the methyl and phenyl groups of the ligands were replaced by hydrogen atoms. When optimizing the geometries of the copper complexes, care was taken to preserve the conformation of the eight-membered rings in the initial compounds. The calculations were done using four different basis sets (B1, B2, B3, B4) of increasing quality, which are described in the Computational details section. The difficulty of accurately optimizing these geometries lies in the weak interaction which may take place between the two copper atoms, but this distance is crucial for any discussion of the metal–metal bonds. Therefore, the capability of reproducing the Cu–Cu distance was used to

Table 6 The calculated and experimental Cu–Cu distances (Å) in complexes $[Cu_2(dppa)_2(NCCH_3)_3]^{2+}$, **2**, and $[Cu_2(dppa)_2(NCCH_3)_4]^{2+}$, **3**

Basis set	$[Cu_2(dppa)_2(NCCH_3)_3]^{2+}$, **2**	$[Cu_2(dppa)_2(NCCH_3)_4]^{2+}$, **3**
B1	3.623	4.258
B2	3.235	3.852
B3	3.013	4.520
B4	3.760	4.225
Exp.	2.869	3.342

check the computational approach. The results are collected in Table 6.

The calculated Cu–Cu distances strongly depend on the type of basis set used and the best agreement between experimental and calculated Cu–Cu distances is not found with the same basis set in both complexes. B3 is the best for **2**, while B2 describes the Cu–Cu distance better for complex **3**. B1 is not expected to provide very good values, owing to the absence of polarization functions, but the reason for the erratic behaviour observed for the other basis sets must lie elsewhere. Indeed, several authors have discussed the inadequacy of DFT methods to describe weak interactions.[14] This applies for dimeric d^{10}–d^{10} complexes in particular, and it has been stated that only MP2 methods can fully provide a good description of such systems. However, MP2 optimization procedures exceed our capabilities. The optimized (B3) and the experimental geometries are shown in Fig. 7 for the two complexes. The conformation of the eight-membered ring is the same in the calculated model and the experimental structure.

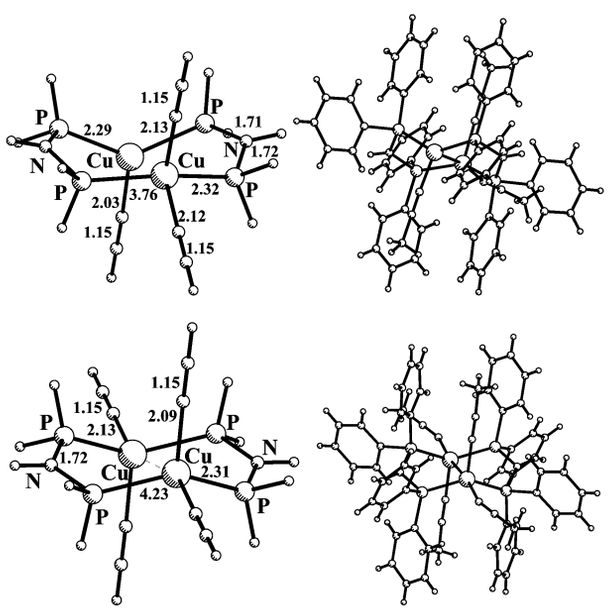

Fig. 7 Comparison between the calculated and experimental structures (distances in Å) of complexes $[Cu_2(dppa)_2(NCCH_3)_3]^{2+}$, **2** (top), and $[Cu_2(dppa)_2(NCCH_3)_4]^{2+}$, **3** (bottom).

The geometry of another member of the series, namely $[Cu_2(dppa)_2(NCCH_3)_2]^{2+}$, the analogue of the Ag complex, was optimized with three basis sets, B2, B3, and B4. Two limiting orientations of the nitrile ligands were considered, *cis* and *trans*. The relative energies of the two isomers, and the Cu–Cu distances are collected in Table 7 for the three basis sets considered.

The spread of distances is large, as happened with the previous examples, but the trends obtained can in principle be trusted. The Cu–Cu increases as nitrile ligands are added, suggesting that the metal–metal interaction is weakened.

The energetics of addition of nitrile ligands to $[Cu_2(dppa)_2(NCCH_3)_2]^{2+}$, to give respectively **2** and **3** was also studied for the formation of the *cis* complexes (ΔE in kcal mol^{-1}). The energy variations for these reactions are much larger than the energy differences between *cis* and *trans* isomers of $[Cu_2(dppa)_2(CH_3CN)_2]^{2+}$, indicating that the result will be essentially the same if the other isomer is considered. The three values given corrrespond to the three basis sets, B2, B3, and B4, respectively.

$$[Cu_2(dppa)_2(HCN)_2]^{2+} + HCN \longrightarrow [Cu_2(dppa)_2(HCN)_3]^{2+},\ \mathbf{2}$$
$$\Delta E = -38.3,\ -17.6,\ -15.8 \text{ kcal mol}^{-1}$$

$$[Cu_2(dppa)_2(HCN)_3]^{2+} + HCN \longrightarrow [Cu_2(dppa)_2(HCN)_4]^{2+},\ \mathbf{3}$$
$$\Delta E = -37.6,\ -20.7,\ -16.0 \text{ kcal mol}^{-1}$$

$$[Cu_2(dppa)_2(HCN)_2]^{2+} + 2HCN \longrightarrow [Cu_2(dppa)_2(HCN)_4]^{2+},\ \mathbf{3}$$
$$\Delta E = -75.9,\ -38.3,\ -31.7 \text{ kcal mol}^{-1}$$

Although the absolute numbers differ, the trends are the same in all cases. The addition reaction is always energetically favored, in agreement with the fact that $[Cu_2(dppa)_2(NCCH_3)_2]^{2+}$ was not observed. The formation of **2** is less favorable than that of **3**, but the retention of one or the other probably depends on the crystallization conditions.

The geometry of the related Ag(I) complexes was also optimized, using a basis set similar to B4 (different only for Ag). Both a model for $[Ag_2(dppa)_2(CH_3CN)_2]^{2+}$, **4**, where Me and Ph groups were replaced by H, as well as $[Ag_2(dppa)_2]^{2+}$, and the dppm analogues were studied. When the phosphine is dppm, the compound formed does not contain nitrile ligands. The calculated and the experimental geometries are shown in Fig. 8.

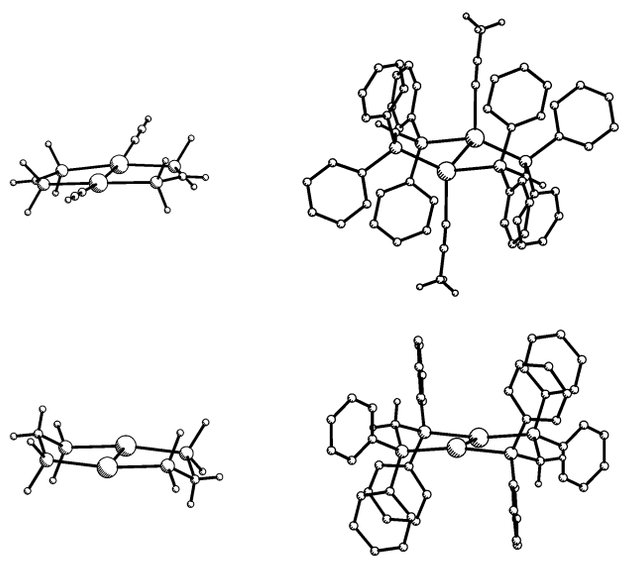

Fig. 8 DFT optimized geometries (left) of models of $[Ag_2(dppa)_2(NCCH_3)_2]^{2+}$, **4** (top), and $[Ag_2(dppm)_2]^{2+}$, **5** (bottom), and X-ray structures (right).

The first striking aspect concerns the effect of the phenyl groups. Indeed, the models exhibit almost planar eight-membered rings, in contrast to the more puckered experimental structures. The effect is more pronounced in the dppa derivative, owing to the presence of the nitrile ligands. In **4**, the nitrile ligands are undoubtly *trans* to each other, while they tend to become almost planar (slightly *cis*) in the model. The calculated Ag–Ag distances are much longer than the experimental ones (3.55, 3.46 Å in the models compared to 2.96 Å in **4**, and 2.95 Å in **5**). As already discussed for the Cu complexes above, the inaccurate description of correlation effects in the DFT method is probably at the origin of this behaviour, although the absence of steric effects from the phenyl rings may be also contributing.

The energetics of addition of two NCH ligands to the $Ag_2(L–L)_2$ frame was calculated for L–L = dppa and dppm. Considering that the model exhibits a relatively different geometry, there is no real difference between the complexes of the two ligands, and the formation of one species or the other may

Table 7 The calculated Cu–Cu distances (Å) in $[Cu_2(dppa)_2(NCCH_3)_2]^{2+}$ for two possible isomers

	cis		*trans*	
Basis set	E/kcal mol^{-1}	d(Cu–Cu)/Å	E/kcal mol^{-1}	d(Cu–Cu)/Å
B2	0.0	3.284	1.5	3.087
B3	0.0	2.719	0.8	2.561
B4	0.0	3.696	2.1	3.561

be more related to experimental conditions than to intrinsic stabilities.

Conclusions

A series of binuclear complexes $[M_2(L–L)_2(NCCH_3)_x]^{n+}$ [M = Cu(I), x = 3, 4; M = Ag(I), x = 2] and dppa was obtained, when working under inert conditions. In the presence of oxygen and Cu(I), the dppa ligand was oxidized, giving rise to an octahedral complex $[Cu(dppaO_2)_3][PF_6]$, **1**, structurally characterized by X-ray diffraction. The M ⋯ M distances in the binuclear complexes increased with the number of nitrile ligands coordinated to each metal. The only well defined M–M bond was found in the silver complex $[Ag_2(dppa)_2(NCCH_3)_2][PF_6]_2$, **4**. In $[Cu_2(dppa)_2(NCCH_3)_3][PF_6]_2$, **2**, there is still a weak bond, which completely disappears in $[Cu_2(dppa)_2(NCCH_3)_4][PF_6]_2$, **3**. These findings were interpreted by DFT calculations. Upon reduction, the binuclear complexes were irreversibly decomposed into the metal.

Experimental

General

Commercially available reagents and all solvents were purchased from standard chemical suppliers. All solvents were used without further purification except acetonitrile (dried over CaH_2) and dichloromethane (dried over CaH_2). The complexes $[M(CH_3CN)_4][PF_6]$ and (M = Cu, Ag) were synthesised according to literature procedures.[15,16] The preparation of the ligands dppa and $dppaO_2$ was based on an existing synthesis route.[17,18]

^{1}H NMR spectra were recorded on a Bruker AMX-300 (300 MHz) spectrometer in d^3-CD_3CN (δ 1.93), using TMS as internal reference, and ^{31}P shifts were measured with respect to external 85% H_3PO_4. Elemental analyses were carried out at ITQB. The IR spectra were recorded on a Unicam Mattson 7000 FTIR spectrometer. Samples were run as KBr pellets.

Syntheses

$[Cu(dppaO_2)_3][PF_6]$, 1. $[Cu(NCCH_3)_4][PF_6]$ (0.186 g, 0.5 mmol) was dissolved in CH_2Cl_2 (10 ml) under nitrogen, and a solution of dppa (0.193 g, 0.5 mmol) in CH_2Cl_2 (10 ml) was added at room temperature. The solution was stirred for 1 h, filtered in air, and one layer of hexane was carefully added to the filtrate. After about three days at room temperature, cubic colourless crystals were formed. A suitable crystal was chosen for single crystal X-ray diffraction. Yield 0.12 g (49% based on dppa). IR (KBr, cm^{-1}): 3291.8 ($\nu_{N–H}$). NMR (CD_3CN): ^{1}H, δ 7.13–7.30 (m, 20H, C_6H_5), 5.04 (s, 1H, N*H*); ^{31}P, δ 38.82 (P from dppa).

$[Cu_2(dppa)_2(NCCH_3)_3][PF_6]_2$, 2, and $[Cu_2(dppa)_2(NCCH_3)_4][PF_6]_2$, 3. $[Cu(NCCH_3)_4][PF_6]$ (0.372 g, 1.0 mmol) was dissolved in CH_2Cl_2 (15 ml) under nitrogen, and a solution of dppa (0.385 g, 1.0 mmol) in CH_2Cl_2 (10 ml) was added at room temperature. The solution became turbid after 2 hours, and a white precipitate formed after 8 hours stirring. The precipitate was filtered, washed with 5 ml of CH_2Cl_2, and dried under vacuum. The yield was 0.45 g.

0.15 g of $[Cu_2(dppa)_2(NCCH_3)_3][PF_6]_2$ were dissolved in 5 ml of $NCCH_3$, from which 0.13 g of $[Cu_2(dppa)_2(NCCH_3)_3][PF_6]_2$ precipitated. Yield 0.12 g (87%). Single crystals (cubic, colorless) suitable for X-ray diffraction were obtained by vapour diffusion of Et_2O into a concentrated $NCCH_3$ solution of the complex at room temperature. Found (calculated for $Cu_2C_{54}H_{51}N_5P_6F_{12}$): C, 48.69 (49.35); H, 3.80 (3.88); N, 5.55 (5.33)%. IR (KBr, cm^{-1}): 3294.6 ($\nu_{N–H}$), 2361.0, 2276.1 ($\nu_{C\equiv N}$). NMR ($NCCD_3N$): ^{1}H, δ 7.32–7.50 (m, 20H, C_6H_5), 5.27 (s, 1H, N*H*); ^{31}P, δ 51.03 (P from dppa).

0.15 g of $[Cu_2(dppa)_2(NCCH_3)_4][PF_6]_2$ were dissolved in 5 ml of $NCCH_3$, from which 0.13 g of $[Cu_2(dppa)_2(NCCH_3)_4][PF_6]_2$ precipitated. Yield 0.12 g (80%). Single crystals (cubic, colorless) suitable for X-ray diffraction were obtained by vapour diffusion of Et_2O into a concentrated $(CH_3)_2CO$ solution of the complex at room temperature. Found (calculated for $Cu_2C_{56}H_{54}N_6P_6F_{12}$): C, 49.75 (47.65); H, 4.03 (4.09); N, 6.22 (4.51)%. IR (KBr, cm^{-1}): 3294.6 ($\nu_{N–H}$); 2361.1, 2276.1 ($\nu_{C\equiv N}$). NMR (CD_3CN): ^{1}H, δ 7.37–7.79 (m, 20H, C_6H_5), 5.33 (s, 1H, N*H*); ^{31}P, δ 46.28 (P from dppa).

$[Ag_2(dppa)_2(NCCH_3)_2][PF_6]_2$, 4. $[Ag(NCCH_3)_4][PF_6]$ (0.208 g, 0.5 mmol) was dissolved in CH_2Cl_2 (10 ml) under nitrogen, and a solution of dppa (0.193 g, 0.5 mmol) in CH_2Cl_2 (10 ml) was added at room temperature. The solution was stirred for 8 h, filtered in air, and one layer of hexane was carefully added to the filtrate. After filtration, hexane was added to the filtrate, and a white precipitate formed. It was filtered, washed with small amounts of hexane several times, and dried *in vacuo*. Yield 0.28 g (82%). Single crystals (cubic, colorless) suitable for X-ray diffraction were obtained by diffusion of hexane into a concentrated CH_2Cl_2 solution of the complex. Found (calculated for $Ag_2C_{52}H_{48}N_4P_6F_{12}$): C, 45.97 (46.65); H, 3.56 (3.58); N, 4.12 (2.80)%. IR (KBr, cm^{-1}): 3286.9 ($\nu_{N–H}$); 2348.8, 2266.5 ($\nu_{C\equiv N}$). NMR ($NCCD_3$): ^{1}H, δ 7.45–7.58 (m, 20H, C_6H_5), 5.72 (s, 1H, N*H*); ^{31}P, δ 59.74, 64.04 (P from dppa).

$[Ag_2(dppm)_2][PF_6]_2$, 5. $[Ag(NCCH_3)_4][PF_6]$ (0.208 g, 0.5 mmol) was dissolved in CH_2Cl_2 (10 ml) under nitrogen, and a solution of dppm (0.193 g, 0.5 mmol) in CH_2Cl_2 (10 ml) was added at room temperature. The solution was stirred for 8 h, and one layer of hexane was carefully added to the filtrate. The white precipitate was filtered, washed with small amounts of hexane several times, and dried in vacuum. Yield 0.27 g (85%). Single crystals (cubic, colorless) suitable for X-ray diffraction were obtained by vapour diffusion of Et_2O into a concentrated $(CH_3)_2CO$ solution of the product. Found (calculated for $AgC_{25}H_{22}P_3F_6$): C, 47.12 (46.70); H, 3.48 (3.61)%. IR (KBr, cm^{-1}): no $\nu_{N–H}$ or $\nu_{C\equiv N}$ bands observed. NMR ($NCCD_3$): ^{1}H, δ 7.29–7.50 (m, 20H, C_6H_5), 3.69–3.73 (m, 2H, CH_2); ^{31}P, δ 9.19, 5.13 (P from dppm).

Crystallography

A summary of the crystallographic data together with data collection and the refinement details for $[Cu(dppaO_2)_3][PF_6]$, **1**, $[Cu_2(dppa)_2(NCCH_3)_3][PF_6]_2$, **2**, $[Cu_2(dppa)_2(NCCH_3)_4][PF_6]_2$, **3**, and $[Ag_2(dppa)_2(NCCH_3)_2][PF_6]_2$, **4**, are given in Table 8.

X-Ray data sets for these four complexes were collected on a MAR research image plate system equipped with graphite-monochromated Mo-Kα radiation (0.71073 Å). 95 frames were

Table 8 Room temperature crystal data and pertinent refinement details for complexes **1**–**4**

	1	**2**	**3**	**4**
Empirical formula	$C_{72}H_{63}CuF_{12}N_3O_6P_8$	$C_{54}H_{51}Cu_2F_{12}N_5P_6$	$C_{62}H_{66}Cu_2F_{12}N_6O_2P_6$	$C_{52}H_{48}Ag_2F_{12}N_4P_6$
M_w	1605.55	1310.90	1468.11	1358.50
Crystal system	Tetragonal	Triclinic	Monoclinic	Monoclinic
Space group	$P4_2/n$	$P\bar{1}$	$P2_1/n$	$P2_1/c$
a/Å	15.857(22)	10.437(15)	14.776(22)	12.845(19)
b/Å	15.857(22)	11.923(15)	14.433(22)	15.362(22)
c/Å	33.280(41)	23.021(32)	17.546(27)	15.613(23)
α/°	(90)	90.32(1)	(90)	(90)
β/°	(90)	94.0(1)	99.34(1)	110.90(1)
γ/°	(90)	90.40(1)	(90)	(90)
V/Å^3	8368(19)	2858(7)	3692(10)	2878(7)
Z	4	2	2	2
D_c/Mg m^{-3}	1.274	1.523	1.321	1.568
μ/mm^{-1}	0.488	0.993	0.779	0.925
Reflections collected	19175	9961	11992	10069
Unique reflections [R(int)]	7424, [0.0691]	9961	6920 [0.0616]	5629 [0.0500]
Final R indices				
R_1, wR_2 [$I > 2\sigma(I)$]	0.1011, 0.2643	0.0774, 0.2039	0.1097, 0.2840	0.0620, 0.1748
R_1, wR_2 (all data)	0.2332, 0.3151	0.1082, 0.2225	0.2088, 0.3393	0.0942, 0.1934

measured at 2° intervals using a counting time appropriate to the crystal under study. Data analysis were performed with the XDS program.[19] No absorption correction was applied to the intensities. The structures were solved by direct methods and refined by full-matrix least-squares method against F^2 using SHELXS and SHELXL from the SHELX-97 package.[20] In complex **3** the unique PF_6^- anion that composed the asymmetric unit was found to be disordered. Two sets of octahedral fluorine atoms were considered and were refined with occupation factors of x and $1 - x$, with x refined to 0.64(2). The phosphorus atom was refined anisotropically while the fluorine atoms were refined with isotropic group thermal parameters. The PF_6^- anion dimensions were constrained in order to give an ideal octahedral geometry. In complex **2** the two PF_6^- anions were also located over two positions and an equivalent model was used to describe the disorder. Refined occupancies for fluorine atoms of 0.54(2) and 0.59(1) in these anions were obtained. In complexes **1** and **4** the PF_6^- anions were refined anisotropically but some temperature factors for fluorine atoms suggest thermal disorder. In the complex cations all the non-hydrogen atoms were refined using anisotropic thermal parameters. However, in complex **1** the carbon atoms of one of the phenyl groups displayed high thermal parameters in one direction, suggesting that it was affected by structural disorder. A trial refinement of a disorder model comprising two alternative positions for this ring (two rigid groups) with refined occupancies was then performed, but didn't lead to a better quality of the final structure. The R values obtained with this disordered model were slightly higher than those listed in Table 8 and the final geometry of the phenyl ring in both orientations was inappropriate in spite of the geometric constraints applied. The C–H hydrogen atoms were inserted in idealised positions and allowed to refine, riding on the parent C atom with an isotropic thermal parameter equal to 1.2 times those to which they were bonded. In complexes **2**, **3** and **4**, the N–H hydrogen atoms of dppa ligands were located from the corresponding difference Fourier maps and subsequently refined with individual isotropic thermal parameters and N–H distances constrained to 0.86 Å. In complex **1**, one crystallographically independent N–H hydrogen was included in a calculated position with a $U_{iso} = 1.2U_{eq}$ of the parent nitrogen, while the remaining one, located from the difference Fourier maps, was included in the refinement using the procedure described above for the N–H hydrogen atoms of the other X-ray structures. The residual electronic densities for complexes **1**, **3** and **4** were within the expected values while the last Fourier map for complex **2** displayed a peak with an electronic density of 1.59 e Å^{-3} which was 0.81 Å within the copper co-ordination sphere. ORTEP diagrams were drawn with PLATON graphical software[21] while the remaining molecular diagrams were performed with the WEBLAB VIEWER[22] graphical software.

CCDC reference numbers 188189–188192.

See http://www.rsc.org/suppdata/dt/b2/b205922n/ for crystallographic data in CIF or other electronic format.

Electrochemistry

All measurements were performed in an acetonitrile solution containing $[NEt_4][PF_6]$ (1.0×10^{-3} mol dm^{-3}) as supporting electrolyte. Anhydrous 99.8% acetonitrile was obtained from Aldrich. Electrochemical grade $[NEt_4][PF_6]$ was purchased from Fluka and used as supplied. Cyclic voltammetry was performed in a three-electrode cell containing a platinum working electrode surrounded by a platinum-spiral counter electrode, and an aqueous saturated calomel reference electrode (SCE) mounted with a Luggin capillary. A BAS 100W electrochemical analyser was used as polarising unit. All the potential values are referenced to the saturated calomel electrode (SCE). Under the present experimental conditions, the one-electron oxidation of ferrocene occurs at $E^{\circ\prime} = +0.38$ V.

Computational details

The geometry optimizations were accomplished by means of *ab initio* and DFT calculations performed with the Gaussian 98 program.[13] The B3LYP hybrid functional[12] was used in all optimizations. That functional includes a mixture of Hartree–Fock[23] exchange with DFT[7] exchange-correlation, given by Becke's three parameter functional[12a] with the Lee, Yang and Parr correlation functional,[12b,c] which includes both local and non-local terms. All the optimized geometries are the result of full optimizations without any symmetry constraints, performed on models with the methyl and phenyl groups replaced by hydrogen atoms. Four basis sets of increasing complexity were used. B1 corresponds to a standard LanL2DZ basis set[24] for all the atoms, B2 represents D95*[24] for C, N and H and LanL2DZ with a d-polarization function for P[25] and an f-polarization function for Cu,[26] B3 is a standard 6-31G**[27] for all atoms and, finally, B4 uses 6-31G** for all atoms except Cu for which the Stuttgart/Dresden effective core potentials with triple zeta valence (SDD)[28] and an added f-polarization function was used.

The extended Hückel calculations[8] were done with the CACAO program[29] and modified H_{ij} values were used.[30] The basis set for the metal atoms consisted of *n*s, *n*p and $(n - 1)$d orbitals. The s and p orbitals were described by single Slater-type wave functions, and the d orbitals were taken as contracted

linear combinations of two Slater-type wave functions. Only s and p orbitals were considered for P. The parameters used for Cu were the following [H_{ii} (eV), ζ]: 4s −11.40, 2.200; 4p −6.06, 2.200; 3d −14.00, 5.950, 2.300 (ζ_2), 0.5933 (C_1), 0.5744 (C_2). Standard parameters were used for other atoms. Calculations were performed on models, $[Cu_2(PH_3)_4(HCN)_n]^{2+}$, n = 3 or 4, based on the experimental structures with idealised maximum symmetry, and the following distances (Å): Cu–Cu 2.80, Cu–P 2.25, Cu–N 2.00, C–N 1.15, C–H 1.08 P–H 1.45. The two metallic moieties, $[Cu(PH_3)_2(NCH)_2]^+$ and $[Cu(PH_3)_2(NCH)_{1/2}]^+$, presented a staggered conformation with 45° L–Cu–Cu–L′ torsion angles, in order to minimize the interligand repulsion, and the ligands on each moiety were bent back 20° (*i.e.*, Cu–Cu–L = 110°) for the same reason.

Acknowledgements

H. L. thanks Praxis XXI for a postdoctoral grant. V. F. thanks FCT for a sabbatical leave grant. The University of Reading and EPSRC are thanked for funds for the Image Plate system. J. N. thanks the Ministry of Education of the Czech Republic (MSM 143100011) for the financial support and NATO Fellowship (ICCTI-01157 22/02/99). M. J. C. and P. Z. gratefully acknowledge the financial support of ICCTI and CNR (in the frame of the Cooperative Programme 2001/2002) and P. Z. the financial support of the University of Siena (PAR 2001). We thank Zara Miravent Tavares for the elemental analysis (ITQB).

References

1 (*a*) P. C. Ford, E. Cariati and J. Bourassa, *Chem. Rev.*, 1999, **99**, 3625; (*b*) V. W.-W. Yam, W. K.-M. Fung and K.-K. Cheung, *Angew. Chem., Int. Ed. Engl.*, 1996, **35**, 1100.
2 J. J. R. Fraústo da Silva and R. J. P. Williams, *The Biological Chemistry of the Elements*, Clarendon Press, Oxford, 1991.
3 (*a*) B. W. Smucker and K. R. Dunbar, *J. Chem. Soc., Dalton Trans.*, 2000, 1309; (*b*) G. Pilloni, B. Corain, M. Degano, B. Longato and G. Zanotti, *J. Chem. Soc., Dalton Trans.*, 1993, 1777; (*c*) H. Börzel, P. Comba, K. S. Hagen, C. Katsichtis and H. Pritzkow, *Chem. Eur. J.*, 2000, **6**, 914.
4 (*a*) S. Kitagawa, H. Maruyama, S. Wada, M. Munukata, M. Nakamura and H. Masura, *Bull. Chem. Soc. Jpn.*, 1991, **64**, 2809; (*b*) M. Maekawa, M. Munukata, S. Kitagawa, T. Kuroda-Sowa, Y. Suenaga and M. Yamamoto, *Inorg. Chim. Acta*, 1998, **271**, 129.
5 (*a*) J. D. Basil, H. H. Murray, J. P. Fackler, Jr., J. Tocher, A. M. Mazany, B. Trzcinska-Bancroft, H. Knachel, D. Dudis, T. J. Delord and D. O. Marler, *J. Am. Chem. Soc.*, 1985, **107**, 6908; (*b*) H. Schmidbaur, *Gold Bull.*, 1990, **23**, 11; (*c*) H. Schmidbaur, *Pure Appl. Chem.*, 1993, **65**, 691.
6 (*a*) L. F. Veiros and M. J. Calhorda, *J. Organomet. Chem.*, 1996, **510**, 71; (*b*) M. J. Calhorda and L. F. Veiros, *J. Organomet. Chem.*, 1994, **478**, 37.
7 R. G. Parr and W. Yang, *Density Functional Theory of Atoms and Molecules*, Oxford University Press, New York, 1989.
8 (*a*) R. Hoffmann, *J. Chem. Phys.*, 1963, **39**, 1397; (*b*) R. Hoffmann and W. N. Lipscomb, *J. Chem. Phys.*, 1962, **36**, 2179.
9 P. Pinto, M. J. Calhorda, V. Félix, T. Avilés and M. G. B. Drew, *Monatsh. Chem.*, 2000, **131**, 1253.
10 B. Ahrens and P. G. Jones, *Acta Crystallogr., Sect. C*, 1998, **50**, 16.
11 F. H. Allen and O. Kennard, *Chem. Des. Autom. News*, 1993, **8**, 31.
12 (*a*) A. D. Becke, *J. Chem. Phys.*, 1993, **98**, 5648; (*b*) C. Lee, W. Yang and R. G. Parr, *Phys. Rev. B*, 1988, **37**, 785; (*c*) B. Miehlich, A. Savin, H. Stoll and H. Preuss, *Chem. Phys. Lett.*, 1989, **157**, 200.
13 Gaussian 98, Revision A.6, M. J. Frisch, G. W. Trucks, H. B. Schlegel, G. E. Scuseria, M. A. Robb, J. R. Cheeseman, V. G. Zakrzewski, J. A. Montgomery, Jr., R. E. Stratmann, J. C. Burant, S. Dapprich, J. M. Millam, A. D. Daniels, K. N. Kudin, M. C. Strain, O. Farkas, J. Tomasi, V. Barone, M. Cossi, R. Cammi, B. Mennucci, C. Pomelli, C. Adamo, S. Clifford, J. Ochterski, G. A. Petersson, P. Y. Ayala, Q. Cui, K. Morokuma, D. K. Malick, A. D. Rabuck, K. Raghavachari, J. B. Foresman, J. Cioslowski, J. V. Ortiz, B. B. Stefanov, G. Liu, A. Liashenko, P. Piskorz, I. Komaromi, R. Gomperts, R. L. Martin, D. J. Fox, T. Keith, M. A. Al-Laham, C. Y. Peng, A. Nanayakkara, C. Gonzalez, M. Challacombe, P. M. W. Gill, B. Johnson, W. Chen, M. W. Wong, J. L. Andres, C. Gonzalez, M. Head-Gordon, E. S. Replogle and J. A. Pople, Gaussian, Inc., Pittsburgh, PA, 1998.
14 (*a*) P. Pyykkö, *Chem. Rev.*, 1997, **97**, 597; (*b*) P. Pyykkö, N. Runeberg and F. Mendizabal, *Chem. Eur. J.*, 1997, **3**, 1451; (*c*) N. Runeberg, M. Schütz and H.-J. Werner, *J. Chem. Phys.*, 1999, **110**, 7210; (*d*) F. A. Cotton and X. Feng, *J. Am. Chem. Soc.*, 1997, **119**, 7514; (*e*) K. Andersson, C. W. Bauschlicher Jr., B. J. Persson and B. O. Roos, *Chem. Phys. Lett.*, 1996, **257**, 238.
15 G. J. Kubas, *Inorg. Synth.*, 1979, **29**, 90.
16 *Organometallic Synthesis*, R. B. King and J. J. Eisch eds., Elsevier, New York, 1986, vol. 3, p. 316.
17 A. Schmidpeter, R. Böhm and H. Groeger, *Angew. Chem., Int. Ed. Engl.*, 1964, **3**, 704.
18 J. D. Woollins, *J. Chem. Soc., Dalton Trans.*, 1996, 2893.
19 W. Kabsch, *J. Appl. Crystallogr.*, 1988, **21**, 916.
20 G. M. Sheldrick, SHELX-97, University of Göttingen, Germany, 1997.
21 A. L. Spek, PLATON, A Multipurpose Crystallographic Tool, Utrecht University, Utrecht, The Nederlands, 1999.
22 WEBLAB VIEWER, version 2.01, Molecular Simulations, Inc., San Diego, 1997.
23 W. J. Hehre, L. Radom, P. v. R. Schleyer and J. A. Pople, *Ab Initio Molecular Orbital Theory*, John Wiley & Sons, NY, 1986.
24 (*a*) T. H. Dunning Jr. and P. J. Hay, *Modern Theoretical Chemistry*, H. F. Schaefer III, ed., Plenum, New York, 1976, vol. 3, p. 1; (*b*) P. J. Hay and W. R. Wadt, *J. Chem. Phys.*, 1985, **82**, 270; (*c*) W. R. Wadt and P. J. Hay, *J. Chem. Phys.*, 1985, **82**, 284; (*d*) P. J. Hay and W. R. Wadt, *J. Chem. Phys.*, 1985, **82**, 2299.
25 A. Höllwarth, M. Böhme, S. Dapprich, A. W. Ehlers, A. Gobbi, V. Jonas, K. F. Köhler, R. Stegmann, A. Veldkamp and G. Frenking, *Chem. Phys. Lett.*, 1993, **208**, 237.
26 A. W. Ehlers, M. Böhme, S. Dapprich, A. Gobbi, A. Höllwarth, V. Jonas, K. F. Köhler, R. Stegmann and A. Veldkamp G. Frenking, *Chem. Phys. Lett.*, 1993, **208**, 111.
27 (*a*) R. Ditchfield, W. J. Hehre and J. A. Pople, *J. Chem. Phys.*, 1971, **54**, 724; (*b*) W. J. Hehre, R. Ditchfield and J. A. Pople, *J. Chem. Phys.*, 1972, **56**, 2257; (*c*) P. C. Hariharan and J. A. Pople, *Mol. Phys.*, 1974, **27**, 209; (*d*) M. S. Gordon, *Chem. Phys. Lett.*, 1980, **76**, 163; (*e*) P. C. Hariharan and J. A. Pople, *Theor. Chim. Acta*, 1973, **28**, 213.
28 (*a*) U. Haeusermann, M. Dolg, H. Stoll and H. Preuss, *Mol. Phys.*, 1993, **78**, 1211; (*b*) W. Kuechle, M. Dolg, H. Stoll and H. Preuss, *J. Chem. Phys.*, 1994, **100**, 7535; (*c*) T. Leininger, A. Nicklass, H. Stoll, M. Dolg and P. Schwerdtfeger, *J. Chem. Phys.*, 1996, **105**, 1052.
29 C. Mealli and D. M. Proserpio, *J. Chem. Educ.*, 1990, **67**, 39.
30 J. H. Ammeter, H.-J. Bürgi, J. C. Thibeault and R. Hoffmann, *J. Am. Chem. Soc.*, 1978, **100**, 3686.